Shot-to-shot electron beam pointing instability in a nonlinear plasma bubble

Bifeng Lei [1,*], Bin Liu [2,†], Mingyuan Shi,[3,4] Andreas Seidel,[3,4] Daniel Seipt [3,4], Matt Zepf,[3,4] and Bin Qiao [1,5,‡]

[1]*Center for Applied Physics and Technology, HEDPS, and SKLNPT, School of Physics, Peking University, Beijing 100871, China*
[2]*Guangdong Institute of Laser Plasma Accelerator Technology, Guangzhou 510415, China*
[3]*Helmholtz-Institute Jena, Fröbelstieg 3, 07743 Jena, Germany*
[4]*Institute of Optics and Quantum Electronics, Max-Wien-Platz 1, 07743 Jena, Germany*
[5]*Frontiers Science Center for Nano-optoelectronic, Peking University, Beijing 100094, China*

Shot-to-shot electron beam pointing instability in the plasma bubble, defined here as electron beam pointing jitter (EBJ), is a long-standing problem that limits the potential of the laser wakefield accelerator (LWFA) in a range of demanding applications. In general, EBJ is caused by variations in laser and plasma parameters from shot to shot, although the exact physical mechanism by which EBJ grows in the plasma wave remains unclear. In this work we theoretically investigate the fundamental physics of EBJ inside the plasma bubble and show how the intrinsic betatron oscillation can act as an amplifier to enhance EBJ growth. The analytical formulas for electron trajectory, pointing angle, and EBJ are derived from the basic momentum equation of an electron and verified numerically. It is shown that the shot-to-shot fluctuations of the laser and plasma parameters, such as laser strength, focus, and carrier-envelope phase, as well as the ambient plasma density and profile, lead to EBJ. The evolution of EBJ is dictated by the dynamics of the plasma bubble. Two amplification processes of the betatron oscillation are found in the rapidly evolving bubbles and play important roles in EBJ growth. The first is driven by a linear resonance in the wobbling bubble due to the coupling of the betatron oscillation and the bubble centroid oscillation. The second is a parametric resonance seen in the breathing bubble, where EBJ grows exponentially due to the strong frequency modulation of the betatron oscillation. Their characteristic functions, growth rates, and resonance conditions are deduced analytically and validated numerically. Finally, we also studied how radiation reaction affects EBJ. Our research provides a clear understanding of the basics of EBJ dynamics in LWFA and will help improve the use of LWFA in demanding applications.

I. INTRODUCTION

The laser wakefield accelerator (LWFA), due to its large acceleration field in order of 100 GV/m in underdense plasma [1], has already been able to produce high-quality low-cost electron beams [2–7] for diverse compact applications [8–12]. In particular, with the breakthrough in plasma bubble excitation [2–4], LWFA experiments can routinely produce high charge ($\sim$nC) [13], high energy (up to 7.8 GeV) [5], low emittance (0.1 mm mrad) [7], low energy spread (0.1 at840 MeV) [6], or high repetition rate [14] electron beams. The recently proposed dephasingless [15] and multistage [16–18] LWFA schemes are expected to push the energy frontier far beyond 10 GeV at the same time with high beam qualities. These efforts will potentially open a path toward their adoption for new applications.

However, for many applications, such as linear collider [19], free-electron laser (FEL), [20] or strong field quantum electrodynamics (SFQED) experiments [21], great efforts are still needed to stabilize the shot-to-shot fluctuations of the accelerated electron beam parameters. For example, a current SFQED experiment essentially requires a GeV electron beam with shot-to-shot $\sim$1 μrad pointing stability and $\sim$1% energy stability to ensure acceptable alignment for collision or diagnostics. Recent work has shown experimentally that the 0.1% shot-to-shot energy stability can be achieved by implementing the well-optimized laser-plasma conditions [22,23] or the hybrid scheme [24] to efficiently reduce the influence of driver fluctuations. However, even with the well-stabilized laser pulse of μrad pointing instability [25,26], the state-of-the-art shot-to-shot electron beam pointing instability (defined here as electron beam jitter, or EBJ) is still at mrad level [27–33]. A significant reduction in EBJ is then highly desirable.

So far numerous experimental efforts have been made to investigate and improve EBJ. Experiments with the Astra laser indicate that EBJ can be mitigated by improving electron injection and laser propagation in the gas jet with the high-contrast ratio laser pulse [34]. In the LLC experiment [27], measurements suggest that the capillary tube is more effective than the gas jet due to smaller shot-to-shot density variations. In the HIJ experiment, it is shown that the stabilization of the carrier-envelope phase (CEP) of the laser pulse is important to mitigate the polarization-dependent EBJ [30]. Other parameters, including laser focus [35] and chirp [36] and plasma

*blei@pku.edu.cn
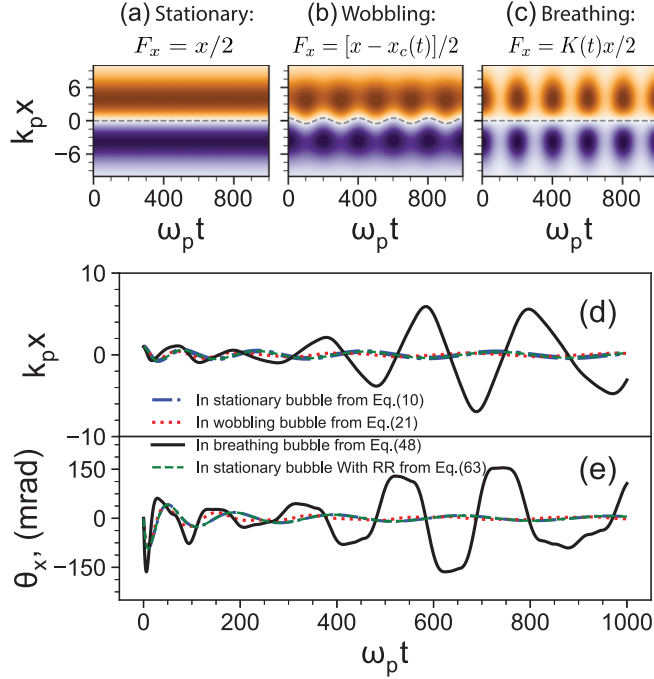†liubin@glapa.cn
‡bqiao@pku.edu.cn

FIG. 1. (a)–(c) Temporal evolution of the transverse focusing force experienced by the trapped electron beam in the stationary, wobbling, and breathing bubble, respectively. The dashed gray line in each plot shows the centroid trajectory of the corresponding bubble. The expressions of the corresponding force F_x, centroid trajectory $x_c(t)$, and strength $K(t)$ of the plasma bubble are discussed in Secs. III–V. (d) Centroid trajectory and (e) pointing angle of an electron beam in the stationary bubble as discussed in Sec. III (dash-dotted blue), in the wobbling bubble as discussed in Sec. IV (dotted red), and in the breathing bubble as discussed in Sec. V (solid black). The dashed green lines present the result in a stationary bubble with the radiation reaction effect considered as discussed in Sec. VI.

density [37], have also been shown to play an important role in EBJ growth. The shot-to-shot variations of these laser and plasma parameters lead to EBJ by influencing the fundamental dynamics of the trapped electron beam in the plasma bubble, e.g., betatron oscillation. Unfortunately, there is still a lack of rigorous experiments delving into the physical mechanisms underpinning EBJ in LWFA. As a result, the dynamics of the trapped electron beam cannot be well understood, especially when the plasma bubble experiences a rapid evolution. For example, the typical evolution processes of the plasma bubble include wobbling during centroid oscillation and breathing during sheath oscillation. The transverse focusing field within the evolving bubble undergoes rapid modulation, as shown in Figs. 1(a)–1(c). This makes a full experimental investigation difficult, as at least hundreds of shots are required to accumulate a sufficient amount of data before a conclusion can be drawn [27,30,33]. Therefore, it is important to understand analytically how the variations of the laser plasma parameters contribute to the growth of EBJ. This understanding will inform the forthcoming experiment.

In this paper we present a theoretical investigation of EBJ in the laser-driven plasma bubble regime, elucidating the underlying mechanisms and the parameter dependence

with analytical formulas. Beginning with the basic equation of motion, we examine the centroid dynamics of the trapped electron beam in a stationary plasma bubble, where the plasma cavity keeps stationary or evolves very slowly in comparison with betatron oscillation. The electron undergoes a linear transverse focusing force that drives a time-dependent harmonic betatron oscillation. It is shown that the betatron dynamics caused by the shot-to-shot initial electron injection jitter in the self-trapping process are the main factors contributing to EBJ growth. Second, EBJ in the wobbling bubble is studied for both a uniform plasma and the preformed plasma channel. The characteristic function of the EBJ growth is derived and its properties are analyzed. It is shown that when the betatron frequency is damped close to the bubble wobble frequency, a linear amplification of the betatron oscillation can be excited, resulting in the linear increase of EBJ during the resonance period. Third, EBJ is found to grow exponentially when the betatron frequency is periodically modulated. This process can act as a highly efficient amplifier of the betatron oscillation. It is therefore crucial that it can be well controlled. Finally, the radiation-damping effect is examined using the Landau-Lifshitz force. The study demonstrates that the radiation reaction can decrease the frequency and amplitude of the betatron oscillation, which subsequently slows the EBJ growth. However, for present LWFA experiments, this effect can be disregarded owing to the weak laser strength.

II. ELECTRON BEAM JITTER (EBJ)

EBJ is measured as the standard deviation of the electron beam pointing angles from shot to shot, for example, in the $\hat{x}$ direction

$$\Delta\theta_{x,J} = \sqrt{\langle\theta_x{}^2\rangle_J - \langle\theta_x\rangle_J^2}, \qquad (1)$$

where $\langle\ldots\rangle_J$ presents the average value over shots. θ_x is the pointing angle of the electron beam in the $\hat{x}$ direction calculated as $\theta_x = \langle p_x/p_z\rangle_b \approx \langle\beta_x\rangle_b$ for an ultrarelativistic electron beam where p_x and p_z present the transverse and longitudinal momentum of an electron inside the beam, respectively, and β_x is the normalized electron velocity. Here $\langle\ldots\rangle_b$ presents the average value over the beam, and the pointing angle θ_x of the beam is calculated from the trajectories as

$$\theta_x = \langle\beta_x\rangle_b = \frac{1}{N_e}\sum_{i=1}^{N_e}\beta_{x,i}, \qquad (2)$$

where $\beta_{x,i}$ presents the normalized velocity of ith electron and N_e the total number of electrons inside the beam. EBJ in the $\hat{y}$ direction, $\Delta\theta_{y,J}$, can be defined in the same way. In two dimensions, the total EBJ can be defined as

$$\Delta\theta_J = \sqrt{\Delta\theta_{x,J}^2 + \Delta\theta_{y,J}^2}. \qquad (3)$$

The physical mechanisms of EBJ growth discussed here are based on the collective centroid dynamics of the trapped electron beam and are identical in both transverse directions. Therefore, for the sake of simplicity, we discuss only the dynamics in the $\hat{x}$ direction in this paper. The $\hat{y}$ direction can also be treated in the same way. The subscript x is therefore dropped, and we denote thereafter $\Delta\theta_J = \Delta\theta_{x,J}$.

As seen from Eqs. (1) and (2), EBJ measures the shot-to-shot variations of the transverse centroid velocity of the trapped electron beam, which is determined by the momentum equation as

$$\left\langle \frac{dp_x}{dt} \right\rangle_b = \langle F_x \rangle_b, \quad (4)$$

where F_x is the transverse force experienced by an electron in the plasma bubble, normalized as $F_x = F_x'/m_e c \omega_p$, where F_x' is the force in CGS unit. In this paper all quantities are normalized by the plasma parameters; e.g., the time is by plasma frequency $\omega_p = \sqrt{4\pi n_0 e^2/m_e}$ and the length by the plasma wave number $k_p = \omega_p/c$. n_0 is the ambient plasma density, m_e mass of electron, c speed of light in vacuum, and e absolute value of electron charge. Equation (4) indicates that the equation of the beam centroid trajectory has the same form as any electron in the beam but with the transverse focusing force $\langle F_x \rangle_b$ experienced by the beam center. The pointing angle of the beam can be calculated as

$$\theta_x = \left\langle \frac{1}{\dot{\gamma}} \left(F_x - \gamma \frac{d^2 x}{dt^2} \right) \right\rangle_b, \quad (5)$$

where γ is the Lorentz factor of an electron. The dot operator denotes the time derivative as $\dot{\gamma} = d\gamma/dt$. According to Eq. (5), the accelerating and focusing forces and the initial conditions of the beam trajectory determine the pointing angle and then EBJ. As a result, there are two physical reasons for the development of EBJ: (1) the shot-to-shot unstable trapping process results in the fluctuation of the initial trajectory conditions and (2) the shot-to-shot instability of the plasma bubble dynamics results in the fluctuation of the focusing and accelerating force. Although in theory both reasons can be attributed to the shot-to-shot fluctuation of the laser and plasma parameters, there are specific physical processes where EBJ increases strikingly. It is therefore important to understand the basic conditions under which such processes occur.

For the electron beam of narrow energy spread $\delta\gamma$, $\delta\dot{\gamma} \ll \langle\gamma\rangle_b$, its centroid trajectory is given from Eq. (4) by

$$\frac{d^2 \langle x \rangle_b}{dt^2} + \alpha \frac{d \langle x \rangle_b}{dt} = \frac{\langle F_x \rangle_b}{\langle \gamma \rangle_b}, \quad (6)$$

where $\alpha = \langle \dot{\gamma}/\gamma \rangle_b$ is the damping coefficient. The pointing angle is calculated by solving Eq. (6) as $\theta_x = d\langle x \rangle_b/dt$. Equation (6) is equivalent to describing the trajectory of an electron residing at the center of the beam, therefore we drop the averaging operator of the beam for the variables (e.g., x, p_x, γ, and F_x) for simplicity in the rest of the paper. Equation (6) can be rewritten to describe the dynamics of this centroid electron as

$$\frac{d^2 x}{dt^2} + \alpha \frac{dx}{dt} = \frac{F_x}{\gamma}. \quad (7)$$

The solution of Eq. (7) consists in principle of two parts: the homogeneous solution determined by the initial conditions and the particular solution determined by the driving force F_x. The initial conditions include the initial injection offset x_0 and angle Θ_0 with respect to the bubble axis, which depends on the initial laser-plasma parameters, e.g., the laser strength a_0, focus w_0, CEP ϕ_{CEP}, or ambient plasma density n_0. In the

different parameter regions, the dynamics of the plasma bubble are distinct as discussed later and can result in the characteristic dynamics of the centroid electron beam, as shown in Fig. 1. As a result, the shot-to-shot variation of these parameters can lead to EBJ. To understand the physics of EBJ and its growth, it is necessary to distinguish these fundamental processes and their dependence on the laser-plasma parameters.

The values of the laser and plasma parameters used for the numerical calculation as shown in Fig. 1 are normalized laser strength, $a_0 = 4$, laser spot size, $w_0 = 4$, laser wavelength, $\lambda_l = 0.8$ μm, initial plasma density, $n_0 = 2.3 \times 10^{18}$ cm^{-3}, and initial Lorentz factor of the trapped electron, $\gamma_0 = 20$. The initial centroid offset of the electron beam is $x_0 = 1$ or $x' = 0.39$ μm and angle $\Theta_0 = 1$ μrad. Unless declared, the values of these parameters are the same as other plots in the following.

Acceleration plays an important role in the centroid dynamics as seen in Eq. (7). The evolution of the Lorentz factor γ is given as

$$\gamma = \gamma_0 + \delta\gamma = \gamma_0 - \int_{t_0}^{t} E_z \, dt' = \gamma_0 + \int_{t_0}^{t} \frac{\zeta}{2} \, dt', \quad (8)$$

where $\gamma_0 = \gamma|_{t=t_0}$ is the Lorentz factor of the electron once it is initially trapped at time $t = t_0$. Here we assume that the electron moves near the bubble axis, and then the longitudinal wakefield $E_z = -\zeta/2$ does not depend on the transverse position [1]. This is typically true for an evacuated plasma bubble which makes the acceleration stable from shot to shot. Unstable acceleration is possible in some cases where, for example, an ultra-high intense laser pulse causes the bubble to break. However, this is not currently of interest in this paper or the LWFA experiments for the ultra-high-quality electron beam. Here ζ is the position of the electron inside the bubble and can be given as $\zeta = \zeta_0 - v_{dp}t$, where ζ_0 is the trapping position and v_{dp} is the dephasing velocity between the electron and the plasma wave. The dephasing velocity in underdense plasma $\gamma_p \gg 1$ can be given as $v_{dp} \simeq 3/2\gamma_p^2$ [38], where $\gamma_p = \omega_l/\omega_p$. ω_l is the laser frequency. As a result,

$$\gamma = \gamma_0 + \frac{\zeta_0}{2}(t - t_0) - \frac{3}{8\gamma_p^2}(t^2 - t_0^2), \quad (9)$$

where the dephasing length is calculated by $\dot{\gamma} = 0$, as $L_d = 2\zeta_0\gamma_p^2/3$. If the initial plasma bubble is spherical with a radius $R = 2\sqrt{a_0}$, the dephasing length is given $L_d = 4\sqrt{a_0}\gamma_p^2/3$ [38], which sets the acceleration limit in the plasma bubble and then the validity of the work presented here.

The energy spread can be estimated from Eq. (9) as

$$\delta\gamma(t) \simeq \sqrt{(\delta\gamma_0)^2 + \frac{\zeta_0\zeta_{\text{eff}}}{4}(\delta t_0)^2 + \frac{(\delta\zeta_0)^2}{4}(t - \langle t_0 \rangle)^2},$$

where $\zeta_{\text{eff}} = \zeta_0 - v_{dp}\delta t_0$ is defined as the effective injection phase of the beam due to dephasing. δt_0 presents the time duration of injection. It is seen that energy spread $\delta\gamma(t)$ depends on the initial energy spread $\delta\gamma_0$, and the phase span $\delta\zeta_0 = v_{dp}\delta t_0$ due to dephasing during the injection process, which is significant in the long-scale injection scheme such as self-injection. A long injection duration is detrimental to the beam quality since it results in a broad energy spectrum

and high emittance. It also prevents Eq. (7) from accurately describing the centroid trajectory of the electron beam. We therefore suppose that the injection of the electron beam into the plasma bubble takes place in a short time, e.g., $\delta t_0 \ll 2\gamma_0/\zeta_0$, and the initial energy spread is small to be insignificant. In this case, the injection of the electron beam into the plasma bubble is minimally affected by the evolution of the laser pulse. Additionally, the beam loading can strongly modify the longitudinal accelerating electric field of the wakefield and increase the energy spread by interplay with injection volume [39]. By properly using a multispecies plasma or tailored density profile a beam loading effect can be used to flatten the accelerating electric field for reducing the energy spread [6,40]. Such strategies will not change the main physics of EBJ as discussed in this paper. For the electron beam with a large energy spread, Eq. (6) becomes

$$\left(1 + \frac{\delta\gamma}{\langle\gamma\rangle_b}\right)\frac{d^2\langle x\rangle_b}{dt^2} + \left(\alpha + \frac{\delta\dot\gamma}{\langle\gamma\rangle_b}\right)\frac{d\langle x\rangle_b}{dt} = \frac{\langle F_x\rangle_b}{\langle\gamma\rangle_b},$$

which is difficult to solve. Therefore, the physics of EBJ in the case of the large energy spread, e.g. due to continuous self-injection or beam loading, is beyond the scope of this paper.

The following is the theoretical discussion of how EBJ develops and evolves in the stationary, wobbling, and breathing bubble with short injection. The physical mechanism leading to the resonance amplification of EBJ growth is found, and the associated conditions are given explicitly.

III. EBJ IN STATIONARY BUBBLE

A stationary bubble is defined here as a fully evacuated plasma bubble whose shape and centroid trajectory remain unchanged or evolve very slowly over time. It is generated by the well-guided laser pulse of moderate strength, e.g., $a_0 \geqslant 2$ [38], and is ideal for high-quality electron beam acceleration. In such a bubble, F_x is linear as $F_x = -x/2$ where the ponderomotive approximation is assumed [41] and the CEP effect is excluded, as shown in Fig. 1(a). Equation (7) becomes

$$\frac{d^2x}{dt^2} + \alpha\frac{dx}{dt} + \omega_\beta^2 x = 0, \tag{10}$$

where $\omega_\beta = 1/\sqrt{2\gamma}$ is the betatron frequency. Equation (10) has the homogeneous solution, referred to here as the time-dependent harmonic betatron oscillation, which depends on the laser strength a_0 and plasma density n_0 due to acceleration as seen in Eq. (9).

In general, EBJ can be calculated from Eq. (10) with the variations of the laser and plasma parameters as shown in Fig. 2, where the betatron oscillation has been smoothed out in Figs. 2(a) and 2(b). The reason is that the betatron oscillation occurs considerably faster than that of EBJ evolution and presents only the kinetic dynamics locally in plasma. Instead, the trend of the amplitude of $\Delta\theta_J$ is of greater significance in characterizing the real measurements in an LWFA experiment. With shot-to-shot variations of up to 20% in a_0 or n_0, EBJ increases to the 0.1 mrad level due to the dephasing effect, which makes the damping effect inefficient with the decreasing α as indicated by Eq. (9). This scales the fluctuation
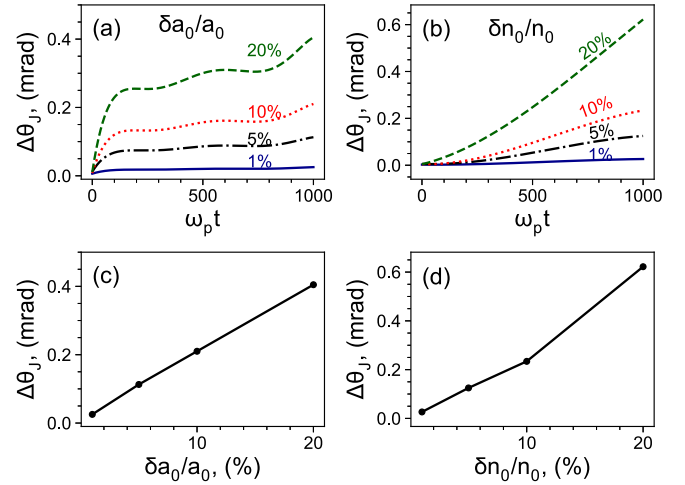

FIG. 2. Evolution of EBJ introduced due to the shot-to-shot variation of laser strength a_0 (a) and plasma density n_0 (b). The relative variations in each plot are 20% (dashed green), 10% (dotted red), 5% (dash-dotted black), and 1% (solid blue) with respect to each stable value. (c), (d) $\Delta\theta_J$ as a function of $\delta a_0/a_0$ and $\delta n_0/n_0$ after propagation $t = 1000$, respectively. EBJ is calculated by the randomly sampled variations in parameters over 100 shots and by smoothing out the betatron oscillation.

tolerance of a_0 and n_0 for the acceptable EBJ in experiments as shown in Figs. 2(c) and 2(d). Other parameters including w_0 and γ_0 make no contribution in this case.

To understand the evolution of EBJ qualitatively, we can solve Eq. (10) analytically. The general form of the solution can be assumed as

$$x(t) = A(t)e^{iS(t)}, \tag{11}$$

where $A(t)$ and $S(t)$ are the time-dependent amplitude and phase, respectively. Its first and second derivatives are given as

$$\dot x = (\dot A + iA\dot S)e^{iS},$$
$$\ddot x = (\ddot A + 2i\dot A\dot S + iA\ddot S - A\dot S^2)e^{iS}.$$

By inserting them into Eq. (10) and collecting real and imaginary parts separately, we obtain the coupled equations as

$$\text{Real:} \quad \ddot A + \alpha\dot A + (\omega_\beta^2 - \dot S^2)A = 0,$$
$$\text{Imaginary:} \quad 2\dot A\dot S + \alpha A\dot S + A\ddot S = 0.$$

By assuming very slow variation of $A(t)$ and $\gamma(t)$ where $|\ddot A| \ll 1$ and $|\alpha\dot A| \ll 1$, from the real part, we obtain

$$\omega_\beta^2 - \dot S^2 = 0, \tag{12}$$

therefore

$$S = \pm\int_{t_0}^{t}\omega_\beta(t')\,dt' = \pm\varphi_\beta(t), \tag{13}$$

where $\varphi_\beta(t)$ is defined as the phase of betatron oscillation. From the imaginary part, it is easy to obtain

$$\frac{1}{A^2\omega_\beta}\frac{d(A^2\omega_\beta)}{dt} = -\frac{\dot\gamma}{\gamma}. \tag{14}$$
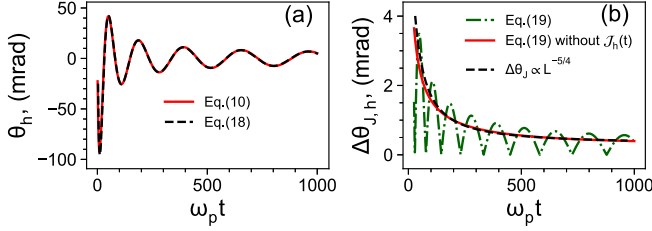
FIG. 3. (a) Temporal evolution of pointing angle θ_x calcualted numerically from Eq. (10) (solid red) and theoretically from Eq. (18) (dashed black). (b) Temporal evolution of EBJ $\Delta\theta_h$ calculated from Eq. (19) with (dash-dotted green) or without (solid red) the fast oscillation term $\mathcal{J}_h(t)$. The scaling law is fit according to Eq. (20) (dashed black). The initial injection jitter of the electron is $\Delta x_0 = 0.3$ and $\Delta\Theta_0 = 1$ μrad. The other laser and plasma parameters are shot-to-shot stable.

As a result,

$$
A(t) = \sqrt{\frac{\gamma_0 \omega_{\beta 0}}{\gamma \omega_\beta}} = \left(\frac{\gamma_0}{\gamma}\right)^{1/4} = e^{-\int_{t_0}^{t} \frac{\alpha(t')}{4} dt'}
$$
$$
= e^{-\frac{1}{4}\int_{t_0}^{t} \frac{d\dot\gamma}{\gamma}} = e^{-\frac{1}{4}\ln\frac{\gamma}{\gamma_0}}, \tag{15}
$$

which represents the betatron damping effect due to acceleration. Now we can write the solution in the form

$$
x(t) = A(t)(C_+ e^{i\varphi_\beta(t)} + C_- e^{-i\varphi_\beta(t)}). \tag{16}
$$

By substituting Eq. (16) into Eq. (10), it is easy to find

$$
C_+ = \frac{1}{2}\left(x_0 - i\frac{\Theta_0}{\omega_{\beta 0}}\right),
$$
$$
C_- = \frac{1}{2}\left(x_0 + i\frac{\Theta_0}{\omega_{\beta 0}}\right),
$$

where x_0 and $\Theta_0 = p_{x0}/\gamma_0$ are the initial position and angle of the electron at the trapping point, respectively. Now the homogeneous solution of Eq. (10) is given as

$$
x_h(t) = A(t)\left(x_0 \cos\varphi_\beta(t) + \frac{\Theta_0}{\omega_{\beta 0}} \sin\varphi_\beta(t)\right). \tag{17}
$$

The pointing angle due to the harmonic betatron oscillation is calculated from Eq. (17) by

$$
\theta_h = A(t)\Gamma(t)\Big(-x_0 \sin[\varphi_\beta(t) + \Psi(t)]
$$
$$
+ \frac{\Theta_0}{\omega_{\beta 0}} \cos[\varphi_\beta(t) + \Psi(t)]\Big), \tag{18}
$$

where $\Gamma(t) = \sqrt{\alpha(t)^2/16 + \omega_\beta^2}$, $\tan\Psi(t) = \alpha(t)/4\omega_\beta(t)$. It is verified by comparing it with the numerical solution of Eq. (10) as shown in Fig. 3(a). θ_h oscillates at the betatron frequency and rapidly grows to approximately ~100 mrad in the beginning, owing to the initial offset x_0. For instance, $\theta_h \simeq 25$ mrad for $x_0 = 1$. Here EBJ is determined by the shot-to-shot variations of initial offset x_0 and angle Θ_0. By inserting

Eq. (18) into Eq. (1), EBJ can be obtained as

$$
(\Delta\theta_h)^2 = \frac{A(t)^2 \Gamma(t)^2}{2}[\mathcal{J}_{h0} - \mathcal{J}_h(t)], \tag{19}
$$

where the initial injection jitter of the electron is defined as $\mathcal{J}_{h0}^2 = (\Delta x_0)^2 + (\Delta\Theta_0)^2/\omega_{\beta 0}^2$. $\Delta x_0 = \sqrt{\langle x_0^2\rangle_J - \langle x_0\rangle_J^2}$ and $\Delta\Theta_0 = \sqrt{\langle\Theta_0^2\rangle_J - \langle\Theta_0\rangle_J^2}$ measure the electron injection instability into the plasma bubble and may be induced during multistage coupling [42] or the unstable trapping process by, for example, the laser pulse jitter, CEP-, tilted laser pulse intensity front-, external magnetic field-, plasma density modulation-, or laser focus-controlled injection [43–48]. The fast oscillation function $\mathcal{J}_h(t)$ is given as

$$
\mathcal{J}_h(t)^2 = \mathcal{J}_{h1}^2 \cos[2\varphi_\beta(t) + 2\Psi(t)]
$$
$$
+ \mathcal{J}_{h2}^2 \sin[2\varphi_\beta(t) + 2\Psi(t)],
$$

where $\mathcal{J}_{h1}^2 = (\Delta x_0)^2 - (\Delta\Theta_0)^2/\omega_{\beta 0}^2$ and $\mathcal{J}_{h2}^2 = (\Delta x_0 \Theta_0)/\omega_{\beta 0}$ presents the correlation between injection offset x_0 and angle Θ_0. Generally, $\mathcal{J}_{h1} \ll \mathcal{J}_{h0}$ and $\mathcal{J}_{h2} = 0$ if there is no correlation between x_0 and Θ_0. As a result, $\mathcal{J}_h(t)$ is not important as shown in Fig. 3(b) by comparing dashed black and sold red lines and can be neglected. EBJ can then be reduced to

$$
\Delta\theta_h \simeq \frac{\mathcal{J}_{h0}}{\sqrt{2}} A(t)\Gamma(t) \propto \mathcal{J}_{h0} L^{-5/4}, \tag{20}
$$

where L is the acceleration distance. The injection jitter-induced EBJ here is in mrad level, which is one order higher than that induced by the direct variation of a_0 or n_0 in Fig. 2. A similar feature can also be seen that $\Delta\theta_h$ is initially very large or $\Delta\theta_h \simeq 5$ mrad even for very small $x_0 = 1$ or $x_0' = 0.8$ μm. This feature implies that optimizing the control of the initial injection offset for the electron beam is more important than adjusting the angle, as the strong focusing force plays a significant role. As the electron beam is accelerated, the coefficient $A(t)$ characterizes a decrease in θ_h. The suppression rate is scaled as $L^{-5/4}$ which should be beneficial from the long-propagation distance. However, the long-scale LWFA faces more serious issues when the plasma bubble rapidly evolves, as discussed later.

IV. EBJ IN TRANSVERSE WOBBLING BUBBLE

A wobbling bubble is defined as an evacuated plasma bubble that undergoes a centroid oscillation. The plasma bubble wobbles transversely when the laser-plasma scattering is asymmetric [49], or the driver pulse undergoes a centroid oscillation [50–53]. The focusing force experienced by the electron depends on the centroid trajectory of the bubble $x_c(t)$ as $F_x = -[x - x_c(t)]/2$ as shown in Fig. 1(b). As a result, the electron undergoes driven harmonic oscillations as

$$
\frac{d^2 x}{dt^2} + \alpha\frac{dx}{dt} + \omega_\beta^2 x = \omega_\beta^2 x_c(t), \tag{21}
$$

where the homogeneous solution of Eq. (21) is the same as Eq. (17). Similarly, the EBJ due to shot-to-shot variations in the laser and plasma parameters can be calculated numerically from Eq. (21). For example, as shown quantitatively in Fig. 4, the variation of w_0 or n_0 leads to mrad-level EBJ in the
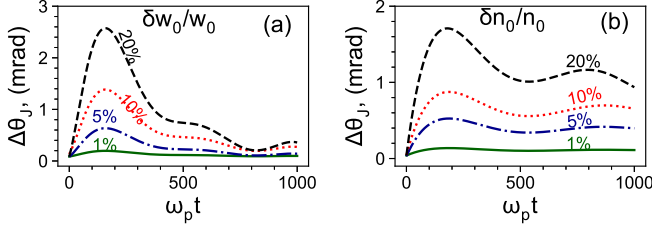
FIG. 4. Temporal evolution of EBJ with 1% (solid green), 5% (dash-dotted blue), 10% (dotted red), and 20% (dashed black) shot-to-shot variation of w_0 (a) and n_0 (b). They are numerically calculated by Eq. (21). The variations in parameters are randomly sampled over 100 shots and the betatron oscillation is smoothed out.

beginning, which is larger than that in the stationary bubble. Other parameters, such as a_0 or γ_0, have negligible effects.

The particular solution of Eq. (21) is given as

$$x_p(t) = 2\omega_{\beta 0} A(t) \int_{t_0}^{t} A(t') x_c(t') \sin[\varphi_\beta(t) - \varphi_\beta(t')] dt', \quad (22)$$

and the corresponding pointing angle is

$$\theta_p = 2\omega_{\beta 0} A(t) \Gamma(t) \int_{t_0}^{t} A(t') x_c(t') g(t, t') dt', \quad (23)$$

where $g(t, t') = -\frac{\alpha(t)}{4} \sin[\varphi(t) - \varphi(t')] + \omega_\beta(t) \cos[\varphi(t) - \varphi(t')]$. According to Eq. (23), the particular pointing angle is independent of the initial injection of the electron and is verified with Eq. (21) as shown in Fig. 5(a). The EBJ can then
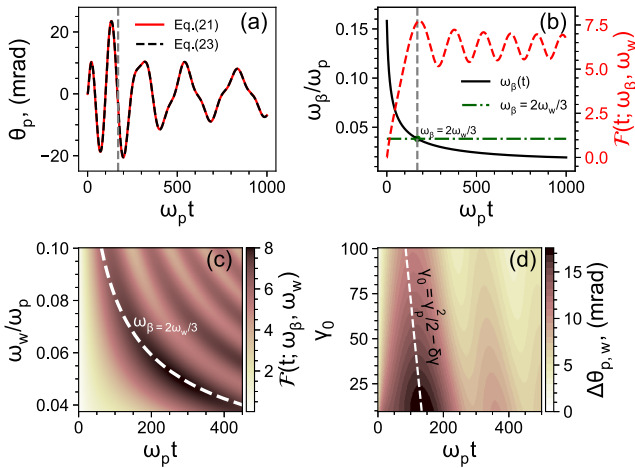

FIG. 5. (a) Temporal evolution of pointing angle θ_p from a particular solution calculated from Eq. (21) (solid red) and Eq. (23) (dashed black). (b) Temporal evolution of Betatron frequency ω_β (solid black) and parametric function $\mathcal{F}(t; \omega_\beta, \omega_w)$ (dashed red). The vertical dashed gray line shows the position where the resonant condition $\omega_\beta \simeq 2\omega_w/3$ (dash-dotted green) is met. (c) Distribution of parametric function $\mathcal{F}(t; \omega_\beta, \omega_w)$ as a function of ω_w during acceleration. (d) Temporal evolution of particular EBJ $\Delta\theta_{p,w}$ with initial Lorentz factor varying in range $10 < \gamma_0 < 100$. The dashed white line shows the resonant position implied by Eq. (32).

be calculated by using the shot-to-shot variation of the bubble centroid trajectory $x_c(t)$, as

$$(\Delta\theta_{p,w})^2 = 4\omega_{\beta 0}^2 A(t)^2 \Gamma(t)^2 \int_{t_0}^{t} \int_{t_0}^{t} A(t')A(t'')$$
$$\times [\Delta x_c(t', t'')]^2 g(t, t') g(t, t'') dt' dt'', \quad (24)$$

where $\Delta x_c(t', t'') = \sqrt{\langle x_c(t')x_c(t'')\rangle_J - \langle x_c(t')\rangle_J \langle x_c(t'')\rangle_J}$.

We now consider the periodically wobbling bubble with a centroid trajectory such as discussed in [30,49] as

$$x_c(t) = x_w(t)\cos(\omega_w t + \phi_w), \quad (25)$$

where the amplitude $x_w(t)$ and the phase ϕ_w are determined by the asymmetry during the laser and plasma interaction. ω_w is the wobble frequency. The bubble can oscillate periodically in two major situations: (1) a CEP-dominated bubble where the transverse momentum transfer from the laser pulse to plasma electrons depends on the phase of the pulse front and evolves periodically, which is significant in the bubble driven by the few-cycle or the front-etched pulse, and (2) a mismatched plasma channel where the off-axis or oblique injection of the laser pulse causes the bubble to oscillate around the channel axis [50,51,54]. The more complex scenario, which is not the focus of the current LWFA studies and will not be covered in this paper, is in the wobbling bubble caused by beating high-order modes, e.g., Hermite-Gaussian (HG) modes [53,55].

By assuming stable wobbling amplitude x_w and frequency ω_w, together with Eq. (25) the centroid jitter of the plasma bubble can be calculated by

$$[\Delta x_c(t', t'')]^2 = x_w(t')x_w(t'')\langle \sin(\omega_w t' + \phi_w)$$
$$\times \sin(\omega_w t'' + \phi_w)\rangle_J - \langle \sin(\omega_w t' + \phi_w)\rangle_J$$
$$\times \langle \sin(\omega_w t'' + \phi_w)\rangle_J. \quad (26)$$

In the CEP-driven case, the bubble wobbles due to the asymmetric scattering of the laser pulse, and the plasma is determined by the laser pulse front phase ζ_f. ω_w can then be calculated from the temporal evolution of ζ_f as $\omega_w = d\zeta_f/dt \simeq \omega_l(v_{ph} - v_g + v_{etch})/\omega_p \sim 1/\gamma_p = \lambda_l/\lambda_p \sim \sqrt{n_0}$ with v_{ph}, v_g and v_{etch} are phase, group, and etching velocity of the laser pulse, respectively. It is $\omega_w \simeq 3/2\gamma_p$ in the bubble region [30,56]. As shown in Ref. [56], the amplitude $x_w(t) \propto a_0\sqrt{n_0}/w_0\tau_f$, where τ_f is the duration of pulse front.

The wobble phase ϕ_w is related to the CEP as $\phi_w = \phi_{CEP} + \phi_{w0}$ where ϕ_{w0} is an arbitrary phase depending on the electron injection and is trivial. As a result, Eq. (26) becomes

$$[\Delta x_c(t', t'')]^2 = x_w(t')x_w(t'')(\cos\omega_w t' \cos\omega_w t'' + \sin\omega_w t' \sin\omega_w t''), \quad (27)$$

where $\langle\sin(\omega_w t' + \phi_w)\rangle_J = 0$, $\langle\sin(\omega_w t'' + \phi_w)\rangle_J = 0$ and $\langle\cos[\omega_w(t' + t'') + 2\phi_w]\rangle_J = 0$ for a large number of shots with unstable CEP. Therefore, EBJ can be calculated from

Eq. (24) as

$$(\Delta\theta_{p,w})^2 = 2\omega_{\beta0}^2 A(t)^2 \Gamma(t)^2$$

$$\times \left(\left[\int_{t_0}^t A(t') x_w(t') \cos\omega_w t' \cos\Phi(t,t') \, dt' \right]^2 \right.$$

$$\left. + \left[\int_{t_0}^t A(t') x_w(t') \sin\omega_w t' \cos\Phi(t,t') \, dt' \right]^2 \right)$$

$$\simeq \omega_{\beta0}^2 x_{w0}^2 A(t)^2 \Gamma(t)^2 \mathcal{F}_0^2(t; \omega_\beta, \omega_w), \tag{28}$$

where $\Phi(t,t') = \psi_\beta(t) - \psi_\beta(t') + \Psi(t)$. Here, the wobble amplitude varies very slowly and is assumed to be constant as $x_w(t) = x_{w0}$. This is reasonable since the steepness of the pulse front is stable for a few-cycle pulse or the pulse front has already been etched [56]. In Eq. (28) we have used an approximation as

$$\left[\int_{t_0}^t A(t') x_w(t') \sin\omega_w t' \cos\Phi(t,t') \, dt' \right]^2$$

$$\simeq \left[\int_{t_0}^t A(t') x_w(t') \cos\omega_w t' \cos\Phi(t,t') \, dt' \right]^2$$

$$\simeq \frac{1}{4} \left| \int_{t_0}^t A(t') e^{i \int (\omega_\beta - \omega_w) dt''} dt' \right|^2$$

$$= \frac{1}{4} \mathcal{F}_0^2(t; \omega_\beta, \omega_w), \tag{29}$$

by neglecting the fast oscillation terms. The parametric function $\mathcal{F}_0(t; \omega_\beta, \omega_w)$ is defined as

$$\mathcal{F}_0(t; \omega_\beta, \omega_w) = \left| \int_{t_0}^t A(t') e^{i \int (\omega_\beta - \omega_w) dt''} dt' \right|, \tag{30}$$

which characterizes the growth of $\Delta\theta_{p,w}$. The linear resonance occurs as the betatron frequency approaches the condition

$$\omega_\beta = \frac{2\omega_w}{3} \tag{31}$$

and cannot be sufficiently suppressed by energy gain, as shown in Figs. 5(b) and 5(c). EBJ grows rapidly to 10 mrad around the resonance points as shown in Fig. 5(d), which is one order higher than the harmonic betatron case as shown in Fig. 3.

The resonance condition in Eq. (31) can be self-matched as ω_β decreases during acceleration as shown in Fig. 5(b), which depends on the energy gain condition as

$$\gamma_0 \simeq \frac{\gamma_p^2}{2} - \delta\gamma. \tag{32}$$

It connects the plasma density to the electron injection energy. It is clear that, if initially $\gamma_0 < \gamma_p^2/2$, the betatron resonance takes place once the energy gain of the trapped electron beam $\delta\gamma$ can approximately meet the condition in Eq. (32). The temporal evolution of the particular EBJ $\Delta\theta_{p,w}$ is shown in Fig. 5(d) with the initial Lorentz factor varying in the range $10 < \gamma_0 < 100$. The white dashed line illustrates the resonance condition in Eq. (32). It is seen that the lower γ_0 which is usually seen in the controlled injection schemes such as by ionization [57], or density transition [58], leads to the larger

EBJ $\Delta\theta_p$ at a later time. This implies that the injection mechanism could potentially regulate $\Delta\theta_p$. In the bubble regime, this resonance tends to occur since γ_p is usually greater than γ_0 in underdense plasma. In practice, the CEP-driven EBJ experiences significant growth in two scenarios. First, the plasma bubble is driven by a few-cycle pulse [49] in a short propagation distance where the laser pulse is well guided by the plasma, and the bubble sheath remains stable. Thus the bubble dynamics can be described by its centroid trajectory in Eq. (25). The second scenario is the front-sharpened laser pulse-driven bubble. With a sharp pulse front exhibiting temporally asymmetric profile [30], the bubble centroid oscillates in response to the phase shifts of the pulse front in relation to CEP.

In theory, the coupling between the wobble-driven oscillation in Eq. (23) and harmonic betatron oscillation in Eq. (18) should result in an extra EBJ. Since

$$\theta = \theta_h + \theta_p, \tag{33}$$

then

$$\Delta\theta_J = \sqrt{(\Delta\theta_h)^2 + (\Delta\theta_p)^2 + 2\Delta\theta_h\theta_p}. \tag{34}$$

As a result, the coupling EBJ is given as

$$\Delta\theta_h\theta_p = \langle\theta_h\theta_p\rangle_J - \langle\theta_h\rangle_J\langle\theta_p\rangle_J. \tag{35}$$

Here it is calculated as

$$\Delta\theta_h\theta_p = 0 \tag{36}$$

because θ_h and θ_p are driven by the independent sources. When there are several modes of bubble centroid oscillations, the coupling EBJ between each mode occurs.

In the preformed plasma channel, the shot-to-shot pointing instability of the laser pulse introduces both the initial injection jitter of the electron beam and the centroid oscillation of the bubble, so they are coupled [42]. Additionally, the dynamics may be more complicated due to the CEP effect, which could result in the above-mentioned bubble wobbling.

First, we consider the bubble wobble in the plasma channel of the matched profile $n_p = n_0 + \Delta n x^2/w_0^2$ considered, where Δn is the matched channel depth [59]. The transverse injection offset x_{l0} or angle Θ_{l0} of the laser pulse with respect to the channel axis can result in the centroid oscillation of the laser pulse and then the plasma bubble [51,60]. The frequency depends on the Rayleigh length Z_R of the laser pulse approximately as $\omega_{ch} = 1/Z_R$. By neglecting the high-order nonlinear effect and assuming a well-controlled CEP, the centroid trajectory of the bubble can be written as

$$x_c(t) = x_{ch}(t) = x_{l0} \cos\omega_{ch}t + Z_R\Theta_{l0} \sin\omega_{ch}t$$

$$= x_{ch0} \cos(\omega_{ch}t + \phi_{ch}), \tag{37}$$

where the amplitude is $x_{ch0} = \sqrt{x_{l0}^2 + Z_R^2\Theta_{l0}^2}$. The phase $\phi_{ch} = \arctan(x_{l0}/Z_R\Theta_{l0})$ is related to the initial injection condition of the laser pulse but not CEP. This leads to the correlation between the betatron oscillation in Eq. (17) and driven oscillation in Eq. (22) and consequently the coupled EBJ in Eq. (34).
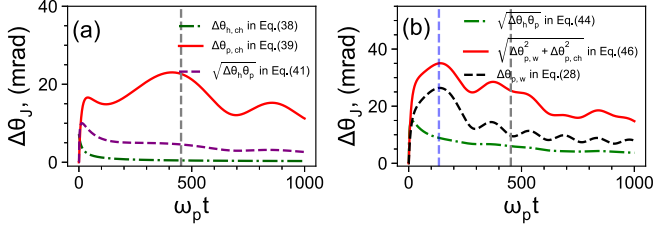
FIG. 6. Temporal evolution of EBJ in a preformed plasma channel under two conditions: (a) the centroid oscillation solely due to channel guiding calculated from Eq. (38), (39), and (41); and (b) the mixed centroid oscillation due to the CEP effect and channel guiding, calculated from Eq. (44), (46), and (28). The vertical dashed lines indicate the positions where $\omega_\beta = 2\omega_w/3$ (dashed blue), and $\omega_\beta = 2\omega_{ch}/3$ (dashed gray). $w_0 = 1.5$ are used. The initial laser jitter is $\Delta x_{l0} = 0.3$, and $\Delta\theta_{l0} = 1$ μrad over 100 random shots.

The homogeneous part is caused by the betatron oscillation in the same form of Eq. (19) as

$$(\Delta\theta_{h,ch})^2 \simeq \tfrac{1}{2}A(t)^2\Gamma(t)^2\mathcal{J}_{ch0}, \tag{38}$$

where the initial laser jitter is defined as $\mathcal{J}_{ch0} = (\Delta x_{l0})^2 + (\Delta\Theta_{l0})^2/\omega_{ch}^2$, and can be controlled well, e.g., under the μrad level in current experiments [26]. The particular part is calculated with the centroid trajectory in Eq. (37) and Eq. (24) as

$$(\Delta\theta_{p,ch})^2 \simeq \omega_{\beta0}^2(\mathcal{J}_{ch0} + \mathcal{J}_{ch1})A(t)^2\Gamma(t)^2\mathcal{F}^2(t;\omega_\beta,\omega_{ch}), \tag{39}$$

where $\mathcal{J}_{ch1} = 2\Delta x_{l0}Z_R\Theta_{l0}$ should be practically small. $\Delta\theta_{p,ch}$ is much larger than $\Delta\theta_{h,ch}$ as shown in Fig. 6(a). The growth of $\Delta\theta_{p,ch}$ is mainly determined by the resonance characterized by $\mathcal{F}(t;\omega_\beta,\omega_{ch})$ around $\omega_\beta = 2\omega_{ch}/3$. The energy gain condition is given as

$$\gamma_0 = \frac{9}{8}Z_R^2 - \delta\gamma \tag{40}$$

and can be flexibly controlled by the laser focus.

Here the bubble centroid oscillation caused by the initial laser jitter is correlated with the harmonic betatron oscillation, giving rise to the coupling EBJ as

$$\Delta\theta_h\theta_p = \omega_{\beta0}A(t)^2\Gamma(t)^2\mathcal{F}(t;\omega_\beta,\omega_{ch})\{\mathcal{J}_{\beta ch0}\cos[\varphi_\beta(t)$$
$$+ \Psi(t) + \varphi_{ch0}] + \mathcal{J}_{\beta ch1}\cos[\varphi_\beta(t) + \Psi(t) + \varphi_{ch1}]\}$$
$$\sim \omega_{\beta0}A(t)^2\Gamma(t)^2\mathcal{F}(t;\omega_\beta,\omega_{ch}). \tag{41}$$

The initial second-order laser jitter is defined as $\mathcal{J}_{\beta ch0} = \sqrt{(\Delta x_{l0})^4 + (\Delta\Theta_{l0})^4/\omega_{\beta0}^2\omega_{ch}^2}$ and $\tan\varphi_{ch0} = \omega_{\beta0}\omega_{ch}(\Delta x_0)^2/(\Delta\Theta_{l0})^2$. The initial laser coupling jitter is introduced by the correlation between the laser injection offset and angle $\mathcal{J}_{\beta ch1} = \sqrt{1/\omega_{\beta0}^2 + 1/\omega_{ch}^2}(\Delta x_{l0}\Theta_{l0})$, which is practically small. $\tan\varphi_{ch1} = \omega_{\beta0}/\omega_{ch}$. It is seen that the coupling EBJ, $\Delta\theta_h\theta_p$, is larger than homogenous EBJ $\Delta\theta_{h,ch}$ but smaller than $\Delta\theta_{p,ch}$ as shown in Fig. 6(a).

The situation becomes more complicated when the CEP effect is also taken into account, which introduces the additional bubble wobble. Assuming that the amplitude of the centroid oscillation due to channel guidance is small compared to the laser spot size, the superposition of these two driven oscilla-

tions of different frequencies is

$$x_c = x_w\cos(\omega_w t + \phi_w) + x_{ch}\cos(\omega_{ch}t + \phi_{ch}), \tag{42}$$

where the subscript w denotes quantities due to the CEP effect. The particular pointing angle is

$$\theta_{p,w,ch} = \theta_{p,w} + \theta_{p,ch}. \tag{43}$$

The homogenous EBJ is the same as Eq. (38). The coupling EBJ in Eq. (35) can also be calculated as

$$\Delta\theta_h\theta_p = \Delta\theta_h(\theta_{p,w} + \theta_{p,ch}) = \Delta\theta_h\theta_{p,w} + \Delta\theta_h\theta_{p,ch}$$
$$\sim \mathcal{F}(t;\omega_\beta,\omega_w) + \mathcal{F}(t;\omega_\beta,\omega_{ch}), \tag{44}$$

where each component in the r.h.s. is in the same form of Eq. (41). The particular EBJ is calculated as

$$(\Delta\theta_{p,w,ch})^2 = (\Delta\theta_{p,w})^2 + (\Delta\theta_{J,p,ch})^2 + 2\Delta\theta_{J,p,w}\theta_{p,ch}. \tag{45}$$

Since there is usually no correlation between CEP and the laser pulse jitter, the coupling term $\Delta\theta_{p,w}\theta_{p,ch}$ in Eq. (45) vanishes. The mixed bubble wobble-driven EBJ can be given as

$$(\Delta\theta_{p,w,ch})^2 = \tfrac{1}{2}\omega_{\beta0}^2A(t)^2\Gamma(t)^2\big[\mathcal{F}^2(t;\omega_\beta,\omega_w)$$
$$+ 2\mathcal{J}_{ch0}^2\mathcal{F}^2(t;\omega_\beta,\omega_{ch})\big], \tag{46}$$

which indicates two resonant points corresponding to $\mathcal{F}(t;\omega_\beta,\omega_{ch})$ and $\mathcal{F}(t;\omega_\beta,\omega_w)$ respectively. It results in a higher EBJ as shown in Fig. 6(b), where the resonance positions are indicated by the blue and gray vertical lines.

The total EBJ in the preformed plasma channel is higher than that in the uniform plasma. This also explains why EBJ can easily become a serious problem in the channel-based LWFA experiments [61]. Each type of centroid oscillation can drive the resonance and wave coupling that contributes to the total EBJ. Therefore, to achieve an EBJ-free electron beam from LWFA, it is essential to appropriately attenuate each type of centroid oscillation.

V. EBJ IN BREATHING BUBBLE

Now we analyze EBJ in a bubble with a deformed sheath, which has been studied and used, for example, in radiation generation [62,63]. The sheath deformation experienced by the trapped electron beam near the bubble axis can be described by a function $K(t)$. As a result, the force can be written by

$$F_x = \frac{K(t)}{2}[x - x_c(t)], \tag{47}$$

where $K(t)$ can be defined in the form of $K(t) = K_B + K_A(t)$. K_B presents the field gradient in the stationary bubble and $K_B = 1$ in an evacuated bubble [64]. $K_A(t)$ presents a perturbation of the focusing force due to the sheath deformation. The equation of motion in Eq. (7) becomes

$$\frac{d^2x}{dt^2} + \alpha\frac{dx}{dt} + \omega_\beta^2K(t)x = \omega_\beta^2K(t)x_c(t), \tag{48}$$

and its solution depends on $K(t)$.

With small deformation where $K_A(t)$ is small or oscillates with a frequency away from the twice betatron frequency
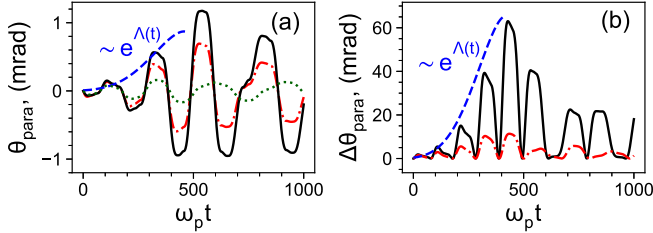
FIG. 7. (a) Evolution of electron pointing angle in a breathing bubble, calculated with $K_E = 1.5$ by Eq. (48) (dash-dotted red) or by Eq. (52) (solid black). The dotted green line shows the case with $K_E = 0.3$ and without the driven term. The dashed blue line is calculated from Eq. (59). (b) Evolution of EBJ in a breathing bubble, calculated by Eq. (48) with $K_E = 1.5$ (solid black) and $K_E = 0.6$ (dash dotted red). The dashed blue line is calculated from Eq. (60). Here the initial EBJ is $\Delta\theta_\alpha = 0.37$ mrad. $\gamma_0 = 200$. The other parameters are the same as above.

ω_β, the homogeneous part of Eq. (48) exists the oscillating solution as

$$x_{h,\text{para}}(t) = A(t)R(t)\left[x_0 \cos\tilde{\varphi}_\beta(t) + \frac{\Theta_0}{\omega_{\beta 0}}\sin\tilde{\varphi}_\beta(t)\right], \quad (49)$$

where $R(t) = [K_0/K(t)]^{1/4}$ and the modulated betatron phase $\tilde{\varphi}_\beta(t) = \int_{t_0}^t \omega_\beta(t')\sqrt{K(t')}\,dt'$. $K_0 = K(t = t_0) = 1$ as the bubble is stable initially. The particular solution is given correspondingly as

$$x_{\text{para}}(t) = \omega_{\beta 0}A(t)R(t)\int_{t_0}^t A(t')R(t')^{-5}x_c(t')$$
$$\times \sin[\varphi_\beta(t) - \varphi_\beta(t')]dt'. \quad (50)$$

As a result, EBJ can be calculated in a similar way as above. The pointing angle and its corresponding EBJ are shown by the dash-dotted red lines in Fig. 7.

With large periodic deformation, the solution becomes dramatically different when the bubble sheath evolves in a breathing manner, as it periodically expands and contracts. As a result, the transverse focusing force experienced by the trapped electron is modulated periodically as shown in Fig. 1(c). We call such a bubble a breathing bubble here. It has been shown that the breathing-like evolution of the bubble is intrinsic in the few-cycle pulse-driven or long-scale LWFA [56]. $K(t)$ can be written in the form as

$$K(t) = K_B + K_E \cos(\omega_b t + \phi_b), \quad (51)$$

where K_E is the amplitude of the sheath deformation. ω_b is the breathing frequency and ϕ_b is the phase. For sufficiently large K_E, Eq. (48) becomes a parametric oscillator where $K(t)$ modulates the betatron frequency ω_β significantly. The oscillator phase locks to the parametric variation and absorbs energy sufficiently if the modulation frequency is close to twice the oscillation frequency $\omega_b \approx 2\omega_\beta$. The amplitude grows exponentially as shown by the black line in Fig. 1. Here the homogeneous part of the betatron oscillation in Eq. (48) dominates the parametric growth as shown by the black and green lines in Fig. 7(a). Equation (48) can be written by

neglecting the damping effect as

$$\frac{d^2x}{dt^2} + \omega_\beta^2[K_B + K_E\cos(\omega_b t + \phi_b)]x = 0. \quad (52)$$

By assuming that the oscillation mode with the frequency away from the resonance frequency does not contribute to the oscillation significantly, the solution can be given in the form as

$$x_{\text{para}}(t) = B_1(t)\cos(\omega_b t/2) + B_2(t)\sin(\omega_b t/2), \quad (53)$$

where $B_1(t)$ and $B_2(t)$ are the time-dependent coefficients. By substituting Eq. (53) into Eq. (52) and neglecting the second derivatives of $B_1(t)$ and $B_2(t)$, it arrives at

$$\begin{bmatrix} dB_1/dt \\ dB_2/dt \end{bmatrix} = \frac{1}{\omega_b}\begin{bmatrix} -\frac{K_E\omega_\beta^2}{2} & \left(\frac{\omega_b^2}{4} - K_B\omega_\beta^2\right) \\ -\left(\frac{\omega_b^2}{4} - K_B\omega_\beta^2\right) & \frac{K_E\omega_\beta^2}{2} \end{bmatrix}\begin{bmatrix} B_1 \\ B_2 \end{bmatrix},$$

which gives the solution

$$B_{1,2} = x_a e^{\eta t}, \quad (54)$$

with the growth rate

$$\eta = \frac{\omega_\beta^2}{\omega_b}\sqrt{K_E^2 - \left(\frac{\omega_b^2}{4\omega_\beta^2} - K_B\right)^2}. \quad (55)$$

Equation (55) indicates a condition with which the exponential solution in Eq. (53) exists, as $K_E \geqslant |\omega_b^2/4\omega_\beta^2 - K_B^2|$. As ω_β decreases with time, it is equivalent to give the range of propagation time only within which the solution (54) is present as shown by the blue lines in Fig. 7(a).

The dominant component of the solution of Eq. (48) is given as

$$x_{\text{para}} \simeq x_a e^{\Lambda(t)}\sin(\omega_b t/2), \quad (56)$$

where x_a is the initial amplitude and $\Lambda(t) = \int_0^t[\eta(t') - \alpha(t')]dt'$. The oscillation amplitude grows exponentially if the damping provided by acceleration cannot compensate for the loss of energy because

$$\eta - \alpha > 0, \quad (57)$$

which indicates the parametric amplification threshold as

$$K_E > K_{ET} = K_B\sqrt{\frac{\alpha^2\omega_w^2}{K_B^2\omega_\beta^4} + \left(\frac{\omega_w^2}{4K_B\omega_\beta^2} - 1\right)^2}. \quad (58)$$

As a result, the parametric amplification of the betatron oscillation can result in exponential growth of EBJ as shown in Fig. 7(b). It subsequently diminishes as the parametric resonance ceases. In principle, the threshold in Eq. (58) is automatically satisfied and fails as the laser pulse propagates in the plasma due to the laser pulse energy depletion and electron energy gain. The corresponding pointing angle and then EBJ can be calculated from Eq. (56) respectively as

$$\theta_{\text{para}} = x_a e^{\Lambda(t)}\left[(\eta - \alpha)\sin(\omega_b t/2) + \frac{\omega_b}{2}\cos(\omega_b t/2)\right] \quad (59)$$

and

$$\Delta\theta_{\text{para}} = \Delta\theta_a \, e^{\Lambda(t)} \left[(\eta - \alpha) \sin(\omega_b t/2) + \frac{\omega_b}{2} \cos(\omega_b t/2) \right],$$

(60)

where $\Delta\theta_a$ presents the initial EBJ prior to parametric oscillation. Even with a slight $\Delta\theta_a$, the parametric betatron oscillation can act as an efficient amplifier, leading to a catastrophic increase in the initial EBJ if the strong sheath oscillation of the plasma bubble significantly modulates the betatron frequency. As shown in Fig. 7(b), with initial $\Delta\theta_\alpha = 0.37$ mrad, EBJ increases by 200 times to 75 mrad after $t = 500$ propagation for $K_E = 1.5$. This is important as the initial EBJ cannot be avoided in LWFA experiments, even if it is exceedingly minimal. However, in the current experiments [5,61,65], this effect is not that bad because the laser is typically used with a long smooth front or the propagation is cut off before getting into serious depletion, where the strength of the bubble hosing is moderate typically as $K_E < 1.0$. As a result, the parametric amplification is weak as seen by the red line in Fig. 7(b), where EBJ grows to 10 mrad for $K_E = 0.6$. However, EBJ will become more notable when using higher intensity lasers, such as the PW lasers, leading to larger K_E. On the other hand, the process of parametric amplification can be used for other purposes, such as to actively manipulate the dynamics of the electron beam or to enhance the betatron radiation by deliberately exciting the bubble breathing with the few-cycle or temporally asymmetric pulse [56].

VI. EBJ DUE TO RADIATION REACTION

As an electron oscillates inside the bubble, it emits the secondary x-ray or γ-ray radiation, which exerts a force acting back on the electron. This kind of force is called the radiation reaction force and can be described classically for a moderate laser strength a_0 [66], as

$$F_{x,RR} = \frac{2r_e}{3} \left\{ \frac{d}{dt} \left(\gamma \frac{dp_x}{dt} \right) + \gamma p_x \left[\left(\frac{d\gamma}{dt} \right)^2 - \left(\frac{dp_x}{dt} \right)^2 \right] \right\},$$

(61)

where $r_e = k_p e^2 / m_e c^2$ is the normalized classical electron radius. Together with the momentum equation in Eq. (4), it arrives at

$$F_{x,RR} = -\alpha_R \frac{dx}{dt} - \frac{r_e}{3} \dot{\gamma} x - \frac{r_e}{6} \gamma^2 x^2 \frac{dx}{dt},$$

(62)

where the radiative damping coefficient is $\alpha_R = r_e(1 - 2\alpha)/3$. As a result, the equation of motion in Eq. (10) is modified to

$$\frac{d^2 x}{dt^2} + (\alpha + \alpha_R) \frac{dx}{dt} + \tilde{\omega}_\beta^2 x = 0,$$

(63)

where the cross-term is not important and neglected. The modified betatron frequency is

$$\tilde{\omega}_\beta = \omega_\beta \sqrt{1 + \frac{2r_e}{3} \dot{\gamma}}.$$

(64)

The solution of Eq. (63) and then EBJ are in the same form as Eqs. (17) and (19), respectively, but with the betatron frequency and damping coefficient modified. As a result, the

radiation reaction suppresses EBJ for the laser pulse $a_0 < \gamma_0^2/4 \sim 100$ from Eq. (9). However, $r_e \sim 10^{-8} \ll 1$ in the typical bubble regime widely considered in current experiments, and therefore, the radiation effect is negligible for the betatron oscillation as shown in Fig. 1 and then for EBJ.

VII. DISCUSSION AND CONCLUSION

Shot-to-shot variation from laser and plasma conditions causes EBJ, the growth of which is regulated by the dynamics of the electron beam in the plasma bubble. We demonstrated in this study that shot-to-shot variations of the initial laser-plasma parameters, including laser strength, focus and CEP, plasma density, and profile, can lead to EBJ, which is dependent on the intrinsic electron dynamics inside the plasma bubble. The injection jitter of the electron beam during the trapping process is the key contributor to EBJ in the stationary bubble, where an electron undergoes a harmonic betatron oscillation. When the bubble wobbles, the centroid oscillation of the bubble determines the EBJ growth and can be characterized by a function $\mathcal{F}(t; \omega_\beta, \omega_w)$ which indicates a linear resonance that can result in significant growth of EBJ. In a preformed plasma channel, EBJ grows much faster due to the coupling between different centroid oscillation modes. A parametric betatron amplification process dominates electron dynamics in a breathing bubble, resulting in the exponential growth of EBJ. It is worth noting that here the growth of EBJ depends on the initial EBJ during the previous injection or propagation section. This makes the effective mitigation of the initial EBJ crucial, which will require more work in both theory and experiment. Finally, we demonstrated that the radiation reaction is advantageous in mitigating EBJ but is negligible in current LWFA.

Through an analytical investigation of plasma bubble dynamics and the physical mechanisms of EBJ, this study provides a qualitative understanding of the beam dynamics and EBJ growth. This knowledge benefits not only EBJ but also the improvement of other beam qualities, such as emittance, energy spread, or phase space optimization since these qualities are also related to the betatron oscillation. Moreover, the quantitative understanding of the parameter dependence, characteristic function, resonance conditions, and threshold can aid in designing experiments to alleviate EBJ or diagnose the beam and bubble dynamics. For instance, by utilizing the resonance condition in Eq. (32), (40), or (58), experimentalists can selectively determine the plasma density, laser focus, and injection scheme to suppress or manipulate the resonance and then the EBJ dynamics.

In addition to LWFA, the high-energy charged particle beam can also drive plasma wakefield acceleration, such as beam-driven plasma wakefield accelerator (PWFA) [67] or hybrid PWFA [68,69]. In such scenarios, the behavior of the plasma bubble can be similar to that observed in LWFA. The trapped electron beam may have the initial injection jitter due to the multistage coupling or driving beam tilt. It is possible that the bubble wobbles in a plasma channel [70] and the bubble sheath is deformed, e.g., when the transverse bunch size of the driving beam is not matched with the plasma density [71]. Therefore, the fundamental physics and EBJ formulation outlined in this paper for LWFA are applicable to PWFA. This

study will help overcome the current constraints of nonlinear plasma bubble-based electron acceleration by enhancing the stability of the plasma bubble and electron beam dynamics. This, in turn, can contribute to potential applications.

[1] E. Esarey, C. B. Schroeder, and W. P. Leemans, Physics of laser-driven plasma-based electron accelerators, Rev. Mod. Phys. **81**, 1229 (2009).

[2] J. Faure, Y. Glinec, A. Pukhov, S. Kiselev, S. Gordienko, E. Lefebvre, J. P. Rousseau, F. Burgy, and V. Malka, A laser–plasma accelerator producing monoenergetic electron beams, Nature (London) **431**, 541 (2004).

[3] C. G. R. Geddes, C. Toth, J. van Tilborg, E. Esarey, C. B. Schroeder, D. Bruhwiler, C. Nieter, J. Cary, and W. P. Leemans, High-quality electron beams from a laser wakefield accelerator using plasma-channel guiding, Nature (London) **431**, 538 (2004).

[4] S. P. D. Mangles, C. D. Murphy, Z. Najmudin, A. G. R. Thomas, J. L. Collier, A. E. Dangor, E. J. Divall, P. S. Foster, J. G. Gallacher, C. J. Hooker *et al.*, Monoenergetic beams of relativistic electrons from intense laser–plasma interactions, Nature (London) **431**, 535 (2004).

[5] A. J. Gonsalves, K. Nakamura, J. Daniels, C. Benedetti, C. Pieronek, T. C. H. de Raadt, S. Steinke, J. H. Bin, S. S. Bulanov, J. van Tilborg *et al.*, Petawatt laser guiding and electron beam acceleration to 8 GeV in a laser-heated capillary discharge waveguide, Phys. Rev. Lett. **122**, 084801 (2019).

[6] L. T. Ke, K. Feng, W. T. Wang, Z. Y. Qin, C. H. Yu, Y. Wu, Y. Chen, R. Qi, Z. J. Zhang, Y. Xu *et al.*, Near-GeV electron beams at a few per-mille level from a laser wakefield accelerator via density-tailored plasma, Phys. Rev. Lett. **126**, 214801 (2021).

[7] G. R. Plateau, C. G. R. Geddes, D. B. Thorn, M. Chen, C. Benedetti, E. Esarey, A. J. Gonsalves, N. H. Matlis, K. Nakamura, C. B. Schroeder *et al.*, Low-emittance electron bunches from a laser-plasma accelerator measured using single-shot x-ray spectroscopy, Phys. Rev. Lett. **109**, 064802 (2012).

[8] J. M. Cole, K. T. Behm, E. Gerstmayr, T. G. Blackburn, J. C. Wood, C. D. Baird, M. J. Duff, C. Harvey, A. Ilderton, A. S. Joglekar *et al.*, Experimental evidence of radiation reaction in the collision of a high-intensity laser pulse with a laser-wakefield accelerated electron beam, Phys. Rev. X **8**, 011020 (2018).

[9] F. Albert and A. G. R. Thomas, Applications of laser wakefield accelerator-based light sources, Plasma Phys. Controlled Fusion **58**, 103001 (2016).

[10] M. Vargas, W. Schumaker, Z.-H. He, K. Behm, V. Chvykov, B. Hou, K. Krushelnick, A. Maksimchuk, J. A. Nees, V. Yanovsky *et al.*, X-ray phase contrast imaging of additive manufactured structures using a laser wakefield accelerator, Plasma Phys. Controlled Fusion **61**, 054009 (2019).

[11] L. Labate, D. Palla, D. Panetta, F. Avella, F. Baffigi, F. Brandi, F. Di Martino, L. Fulgentini, A. Giulietti, P. Köster *et al.*, Toward an effective use of laser-driven very high energy electrons for radiotherapy: Feasibility assessment of multi-field and intensity modulation irradiation schemes, Sci. Rep. **10**, 17307 (2020).

[12] J. M. Cole, D. R. Symes, N. C. Lopes, J. C. Wood, K. Poder, S. Alatabi, S. W. Botchway, P. S. Foster, S. Gratton, S. Johnson *et al.*, High-resolution μCT of a mouse embryo using a compact laser-driven x-ray betatron source, Proc. Natl. Acad. Sci. USA **115**, 6335 (2018).

[13] J. Götzfried, A. Döpp, M. F. Gilljohann, F. M. Foerster, H. Ding, S. Schindler, G. Schilling, A. Buck, L. Veisz, and S. Karsch, Physics of high-charge electron beams in laser-plasma wakefields, Phys. Rev. X **10**, 041015 (2020).

[14] J. Faure, D. Gustas, D. Guénot, A. Vernier, F. Böhle, M. Ouillé, S. Haessler, R. Lopez-Martens, and A. Lifschitz, A review of recent progress on laser-plasma acceleration at kHz repetition rate, Plasma Phys. Controlled Fusion **61**, 014012 (2019).

[15] J. P. Palastro, J. L. Shaw, P. Franke, D. Ramsey, T. T. Simpson, and D. H. Froula, Dephasingless laser wakefield acceleration, Phys. Rev. Lett. **124**, 134802 (2020).

[16] J. Luo, M. Chen, W. Y. Wu, S. M. Weng, Z. M. Sheng, C. B. Schroeder, D. A. Jaroszynski, E. Esarey, W. P. Leemans, W. B. Mori, and J. Zhang, Multistage coupling of laser-wakefield accelerators with curved plasma channels, Phys. Rev. Lett. **120**, 154801 (2018).

[17] Y. Wu, J. Hua, Z. Zhou, J. Zhang, S. Liu, B. Peng, Y. Fang, X. Ning, Z. Nie, F. Li *et al.*, High-throughput injection–acceleration of electron bunches from a linear accelerator to a laser wakefield accelerator, Nat. Phys. **17**, 801 (2021).

[18] C. A. Lindstrøm, Staging of plasma-wakefield accelerators, Phys. Rev. Accel. Beams **24**, 014801 (2021).

[19] C. B. Schroeder, E. Esarey, C. G. R. Geddes, C. Benedetti, and W. P. Leemans, Physics considerations for laser-plasma linear colliders, Phys. Rev. ST Accel. Beams **13**, 101301 (2010).

[20] W. Wang, K. Feng, L. Ke, C. Yu, Y. Xu, R. Qi, Y. Chen, Z. Qin, Z. Zhang, M. Fang *et al.*, Free-electron lasing at 27 nanometres based on a laser wakefield accelerator, Nature (London) **595**, 516 (2021).

[21] M. Turner, S. S. Bulanov, C. Benedetti, A. J. Gonsalves, W. P. Leemans, K. Nakamura, J. van Tilborg, C. B. Schroeder, C. G. R. Geddes, and E. Esarey, Strong-field QED experiments using the BELLA PW laser dual beamlines, Eur. Phys. J. D **76**, 205 (2022).

[22] A. Ferran Pousa, I. Agapov, S. A. Antipov, R. W. Assmann, R. Brinkmann, S. Jalas, M. Kirchen, W. P. Leemans, A. R. Maier, A. Martinez de la Ossa *et al.*, Energy compression and stabilization of laser-plasma accelerators, Phys. Rev. Lett. **129**, 094801 (2022).

[23] G. Loisch, J. Engel, M. Gross, M. Hochberg, H. Huck, G. Koss, O. Lishilin, A. Oppelt, S. Philipp, D. Richter *et al.*, Jitter mitigation in low density discharge plasma cells for wakefield accelerators, J. Appl. Phys. **125**, 063301 (2019).

[24] F. M. Foerster, A. Döpp, F. Haberstroh, K. v. Grafenstein, D. Campbell, Y.-Y. Chang, S. Corde, J. P. Couperus Cabadağ, A. Debus, M. F. Gilljohann *et al.*, Stable and high-quality electron beams from staged laser and plasma wakefield accelerators, Phys. Rev. X **12**, 041016 (2022).

[25] G. Genoud, F. Wojda, M. Burza, A. Persson, and C.-G. Wahlström, Active control of the pointing of a multi-terawatt laser, Rev. Sci. Instrum. **82**, 033102 (2011).

[26] K. Nakamura, H.-S. Mao, A. J. Gonsalves, H. Vincenti, D. E. Mittelberger, J. Daniels, A. Magana, C. Toth, and W. P. Leemans, Diagnostics, control and performance parameters for the bella high repetition rate petawatt class laser, IEEE J. Quantum Electron. **53**, 1 (2017).

[27] F. Desforges, M. Hansson, J. Ju, L. Senje, T. Audet, S. Dobosz-Dufrénoy, A. Persson, O. Lundh, C.-G. Wahlström, and B. Cros, Reproducibility of electron beams from laser wakefield acceleration in capillary tubes, Nucl. Instrum. Methods Phys. Res. A **740**, 54 (2014).

[28] M. Vargas, W. Schumaker, Z. He, Z. Zhao, K. Behm, V. Chvykov, B. Hou, K. Krushelnick, A. Maksimchuk, V. Yanovsky, and A. G. R. Thomas, Improvements to laser wakefield accelerated electron beam stability, divergence, and energy spread using three-dimensional printed two-stage gas cell targets, Appl. Phys. Lett. **104**, 174103 (2014).

[29] A. J. Gonsalves, K. Nakamura, J. Daniels, H.-S. Mao, C. Benedetti, C. B. Schroeder, C. Tóth, J. van Tilborg, D. E. Mittelberger, S. S. Bulanov *et al.*, Generation and pointing stabilization of multi-GeV electron beams from a laser plasma accelerator driven in a pre-formed plasma waveguide), Phys. Plasmas **22**, 056703 (2015).

[30] A. Seidel, B. Lei, C. Zepter, M. C. Kaluza, A. Saevert, M. Zepf, and D. Seipt, Polarization dependent beam pointing jitter in laser wake field accelerators, arXiv:2206.06133 [Phys. Rev. Res. (to be published)].

[31] S. Bohlen, J. C. Wood, T. Brümmer, F. Grüner, C. A. Lindström, M. Meisel, T. Staufer, R. D'Arcy, K. Põder, and J. Osterhoff, Stability of ionization-injection-based laser-plasma accelerators, Phys. Rev. Accel. Beams **25**, 031301 (2022).

[32] J. Huijts, L. Rovige, I. A. Andriyash, A. Vernier, M. Ouillé, J. Kaur, Z. Cheng, R. Lopez-Martens, and J. Faure, Waveform control of relativistic electron dynamics in laser-plasma acceleration, Phys. Rev. X **12**, 011036 (2022).

[33] M. Kirchen, S. Jalas, P. Messner, P. Winkler, T. Eichner, L. Hübner, T. Hülsenbusch, L. Jeppe, T. Parikh, M. Schnepp, and A. R. Maier, Optimal beam loading in a laser-plasma accelerator, Phys. Rev. Lett. **126**, 174801 (2021).

[34] S. P. D. Mangles, A. G. R. Thomas, M. C. Kaluza, O. Lundh, F. Lindau, A. Persson, Z. Najmudin, C.-G. Wahlström, C. D. Murphy, C. Kamperidis *et al.*, Effect of laser contrast ratio on electron beam stability in laser wakefield acceleration experiments, Plasma Phys. Controlled Fusion **48**, B83 (2006).

[35] S. Corde, C. Thaury, A. Lifschitz, G. Lambert, K. Ta Phuoc, X. Davoine, R. Lehe, D. Douillet, A. Rousse, and V. Malka, Observation of longitudinal and transverse self-injections in laser-plasma accelerators, Nat. Commun. **4**, 1501 (2013).

[36] N. A. M. Hafz, T. J. Yu, S. K. Lee, T. M. Jeong, J. H. Sung, and J. Lee, Controlling the pointing angle of a relativistic electron beam in a weakly-nonlinear laser wakefield accelerator, Appl. Phys. Express **3**, 076401 (2010).

[37] S. Li, N. A. M. Hafz, M. Mirzaie, X. Ge, T. Sokollik, M. Chen, Z. Sheng, and J. Zhang, Stable laser–plasma accelerators at low densities, J. Appl. Phys. **116**, 043109 (2014).

[38] W. Lu, M. Tzoufras, C. Joshi, F. S. Tsung, W. B. Mori, J. Vieira, R. A. Fonseca, and L. O. Silva, Generating multi-GeV electron bunches using single stage laser wakefield acceleration in a 3D nonlinear regime, Phys. Rev. ST Accel. Beams **10**, 061301 (2007).

[39] C. Rechatin, X. Davoine, A. Lifschitz, A. B. Ismail, J. Lim, E. Lefebvre, J. Faure, and V. Malka, Observation of beam loading in a laser-plasma accelerator, Phys. Rev. Lett. **103**, 194804 (2009).

[40] G. Li, Q. Ain, S. Li, M. Saeed, D. Papp, C. Kamperidis, and N. A. M. Hafz, Control of electron beam energy-spread by beam loading effects in a laser-plasma accelerator, Plasma Phys. Controlled Fusion **62**, 055004 (2020).

[41] I. Kostyukov, A. Pukhov, and S. Kiselev, Phenomenological theory of laser-plasma interaction in "bubble" regime, Phys. Plasmas **11**, 5256 (2004).

[42] M. Thévenet, R. Lehe, C. B. Schroeder, C. Benedetti, J.-L. Vay, E. Esarey, and W. P. Leemans, Emittance growth due to misalignment in multistage laser-plasma accelerators, Phys. Rev. Accel. Beams **22**, 051302 (2019).

[43] J. Kim, T. Wang, V. Khudik, and G. Shvets, Subfemtosecond wakefield injector and accelerator based on an undulating plasma bubble controlled by a laser phase, Phys. Rev. Lett. **127**, 164801 (2021).

[44] G.-B. Zhang, M. Chen, D.-B. Zou, X.-Z. Zhu, B.-Y. Li, X.-H. Yang, F. Liu, T.-P. Yu, Y.-Y. Ma, and Z.-M. Sheng, Carrier-envelope-phase-controlled acceleration of multicolored attosecond electron bunches in a millijoule-laser-driven wakefield, Phys. Rev. Appl. **17**, 024051 (2022).

[45] A. Popp, J. Vieira, J. Osterhoff, Z. Major, R. Hörlein, M. Fuchs, R. Weingartner, T. P. Rowlands-Rees, M. Marti, R. A. Fonseca *et al.*, All-optical steering of laser-wakefield-accelerated electron beams, Phys. Rev. Lett. **105**, 215001 (2010).

[46] S. R. Yoffe, B. Ersfeld, M. P. Tooley, A. Noble, R. Fraser, and D. A. Jaroszynski, Controlled generation of ultra-short electron bunches using density modulation, in *Relativistic Plasma Waves and Particle Beams as Coherent and Incoherent Radiaon Sources III*, *Proceedings of SPIE*, Vol. 11036, edited by D. Jaroszynski and M. Hur (SPIE, Prague, 2019).

[47] G. Golovin, S. Chen, N. Powers, C. Liu, S. Banerjee, J. Zhang, M. Zeng, Z. Sheng, and D. Umstadter, Independent control of laser wakefield-accelerated electron-beam parameters, in *Laser Acceleration of Electonrs, Protons, and IOns III; and Medical Applications of Laser-Generated Beams of Particles III*,

Proceedings of SPIE, Vol. 9415, edited by K. Ledingham, E. Esarey, K. Spohr, C. Schroeder, P. McKenna, F. Gruner, and P. Bolton (SPIE, Prague, 2015).

[48] T. Matsuoka, C. McGuffey, P. G. Cummings, S. S. Bulanov, V. Chvykov, F. Dollar, Y. Horovitz, G. Kalintchenko, K. Krushelnick, P. Rousseau *et al.*, On electron betatron motion and electron injection in laser wakefield accelerators, Plasma Phys. Controlled Fusion **56**, 084009 (2014).

[49] E. N. Nerush and I. Y. Kostyukov, Carrier-envelope phase effects in plasma-based electron acceleration with few-cycle laser pulses, Phys. Rev. Lett. **103**, 035001 (2009).

[50] S. G. Rykovanov, J. W. Wang, V. Y. Kharin, B. Lei, C. B. Schroeder, C. G. R. Geddes, E. Esarey, and W. P. Leemans, Tunable polarization plasma channel undulator for narrow bandwidth photon emission, Phys. Rev. Accel. Beams **19**, 090703 (2016).

[51] M. Chen, J. Luo, F.-Y. Li, F. Liu, Z.-M. Sheng, and J. Zhang, Tunable synchrotron-like radiation from centimeter scale plasma channels, Light Sci. Appl. **5**, e16015 (2016).

[52] B. Lei, J. Wang, V. Kharin, M. Zepf, and S. Rykovanov, γ-ray generation from plasma wakefield resonant wiggler, Phys. Rev. Lett. **120**, 134801 (2018).

[53] B. Lei, T. Teter, J. W. Wang, V. Y. Kharin, C. B. Schroeder, M. Zepf, and S. G. Rykovanov, Flexible x-ray source with tunable polarization and orbital angular momentum from Hermite-Gaussian laser modes driven plasma channel wakefield, Phys. Rev. Accel. Beams **22**, 071302 (2019).

[54] B. Lei, D. Seipt, M. Shi, B. Liu, J. Wang, M. Zepf, and S. G. Rykovanov, Relativistic modified Bessel-Gaussian beam generated from plasma-based beam braiding, Phys. Rev. A **104**, L021501 (2021).

[55] J. W. Wang, C. B. Schroeder, R. Li, M. Zepf, and S. G. Rykovanov, Plasma channel undulator excited by high-order laser modes, Sci. Rep. **7**, 16884 (2017).

[56] B. Lei, D. Seipt, B. Liu, M. Zepf, and B. Qiao, Parametric amplification of betatron oscillation by bubble breathing in laser wakefield accelerator, arXiv:2303.09389.

[57] M. Chen, E. Esarey, C. B. Schroeder, C. G. R. Geddes, and W. P. Leemans, Theory of ionization-induced trapping in laser-plasma accelerators, Phys. Plasmas **19**, 033101 (2012).

[58] C. Thaury, E. Guillaume, A. Lifschitz, K. Ta Phuoc, M. Hansson, G. Grittani, J. Gautier, J. P. Goddet, A. Tafzi, O. Lundh, and V. Malka, Shock assisted ionization injection in laser-plasma accelerators, Sci. Rep. **5**, 16310 (2015).

[59] C. G. R. Geddes, C. Toth, J. van Tilborg, E. Esarey, C. B. Schroeder, J. Cary, and W. P. Leemans, Guiding of relativistic

laser pulses by preformed plasma channels, Phys. Rev. Lett. **95**, 145002 (2005).

[60] S. G. Rykovanov, C. B. Schroeder, E. Esarey, C. G. R. Geddes, and W. P. Leemans, Plasma undulator based on laser excitation of wakefields in a plasma channel, Phys. Rev. Lett. **114**, 145003 (2015).

[61] W. P. Leemans, A. J. Gonsalves, H.-S. Mao, K. Nakamura, C. Benedetti, C. B. Schroeder, C. Tóth, J. Daniels, D. E. Mittelberger, S. S. Bulanov *et al.*, Multi-GeV electron beams from capillary-discharge-guided subpetawatt laser pulses in the self-trapping regime, Phys. Rev. Lett. **113**, 245002 (2014).

[62] Y. Ma, L. Chen, D. Li, W. Yan, K. Huang, M. Chen, Z. Sheng, K. Nakajima, T. Tajima, and J. Zhang, Generation of femtosecond gamma-ray bursts stimulated by laser-driven hosing evolution, Sci. Rep. **6**, 30491 (2016).

[63] R. Rakowski, P. Zhang, K. Jensen, B. Kettle, T. Kawamoto, S. Banerjee, C. Fruhling, G. Golovin, D. Haden, M. S. Robinson *et al.*, Transverse oscillating bubble enhanced laser-driven betatron x-ray radiation generation, Sci. Rep. **12**, 10855 (2022).

[64] W. Lu, C. Huang, M. Zhou, W. B. Mori, and T. Katsouleas, Nonlinear theory for relativistic plasma wakefields in the blowout regime, Phys. Rev. Lett. **96**, 165002 (2006).

[65] W. P. Leemans, B. Nagler, A. J. Gonsalves, C. Tóth, K. Nakamura, C. G. R. Geddes, E. Esarey, C. B. Schroeder, and S. M. Hooker, GeV electron beams from a centimetre-scale accelerator, Nat. Phys. **2**, 696 (2006).

[66] M. Tamburini, F. Pegoraro, A. D. Piazza, C. H. Keitel, and A. Macchi, Radiation reaction effects on radiation pressure acceleration, New J. Phys. **12**, 123005 (2010).

[67] P. Chen, J. M. Dawson, R. W. Huff, and T. Katsouleas, Acceleration of electrons by the interaction of a bunched electron beam with a plasma, Phys. Rev. Lett. **54**, 693 (1985).

[68] B. Hidding, T. Königstein, J. Osterholz, S. Karsch, O. Willi, and G. Pretzler, Monoenergetic energy doubling in a hybrid laser-plasma wakefield accelerator, Phys. Rev. Lett. **104**, 195002 (2010).

[69] T. Kurz, T. Heinemann, M. F. Gilljohann, Y. Y. Chang, J. P. Couperus Cabadağ, A. Debus, O. Kononenko, R. Pausch, S. Schöbel, R. W. Assmann *et al.*, Demonstration of a compact plasma accelerator powered by laser-accelerated electron beams, Nat. Commun. **12**, 2895 (2021).

[70] Y. Golian and D. Dorranian, Proton driven plasma wakefield generation in a parabolic plasma channel, J. Theor. Appl, Phys, **11**, 27 (2017).

[71] P. Muggli, Beam-driven, Plasma-based particle accelerators, in *CAS-CERN Accelerator School: Plasma Wake Acceleration* (CERN, Geneva, 2016), pp. 119–142.